Double "Mn^{3+}" Stripes in $Bi_{1-x}Sr_xMnO_3$: New Type of Charge Ordering at Room Temperature

M. Hervieu, A. Maignan, C. Martin, N. Nguyen, and B. Raveau*

Laboratoire CRISMAT, UMR 6508 associée au CNRS, ISMRA, 6 bd. Maréchal Juin, 14050 Caen Cedex, France

Received November 2, 2000. Revised Manuscript Received January 31, 2001

The electron microscopy study of the manganites $Bi_{1-x}Sr_xMnO_3$, especially for $x = 1/2$ and $x = 2/3$, has allowed a new type of modulated structure, correlated to charge ordering (CO) phenomena, to be evidenced. The $Bi_{1-x}Sr_xMnO_3$ manganites are characterized by a modulated structure, the modulation vector being qa* ($q \approx 1 - x$), and the I-type symmetry of the perovskite subcell. A model is proposed: the structure can be described by double Mn^{3+} stripes alternating with double ($x = 1/2$) or with quadruple ($x = 2/3$) Mn^{4+} stripes. This type of ordering, observed at room temperature (RT), is compared to that observed in the manganites $Ln_{1-x}Ca_xMnO_3$ at low temperature and in $Bi_{1-x}Ca_xMnO_3$ at RT. The absence of magnetoresistance up to 7*T* suggests that the CO state of $Bi_{0.5}Sr_{0.5}MnO_3$ is exceptionally stable, with a very high T_{CO} close to 500 K. The electron diffraction study carried out versus *T* shows that the superstructure disappears at 500 K and that the phenomenon is reversible.

Introduction

Charge ordering (CO) is a phenomenon of exceptional importance in perovskite manganites, since it implies specific magnetic and transport properties and influences the colossal magnetoresistance (CMR) properties of these materials[1]. CO was observed long ago in manganites $La_{1-x}Ca_xMnO_3$,[2,3] but the possibility to melt the CO state under a magnetic field was only considered recently.[4] At room temperature (RT), all the $Ln_{0.5}Ca_{0.5}MnO_3$ compounds exhibit an orthorhombic *Pnma* perovskite cell, corresponding to a $a^-b^+a^-$ tilting of the octahedra. Charge and orbital ordering, occurring at low temperature, has been especially studied in these manganites with A = La, Nd, Pr, Sm,[5−10] which exhibit a CE-type antiferro-magnetic (AFM) structure. In these oxides, which exhibit an orthorhombic *Pnma* structure (with the cell parameters = "$a_p\sqrt{2} \times 2a_p \times a_p\sqrt{2}$") at RT, the CO state appears at low temperature, that is characterized by a doubling of the **a** parameter. It was proposed that the 1:1 ordering of Mn^{3+} and Mn^{4+} species corresponds to the alternation of single Mn^{3+} and Mn^{4+} stripes along $\vec{a}$ (Figure 1a), concomitantly with an ordering of the Mn^{3+} d_{z^2} orbitals. In fact, the $x = 1/2$ compounds are not the only charge ordered manganites.

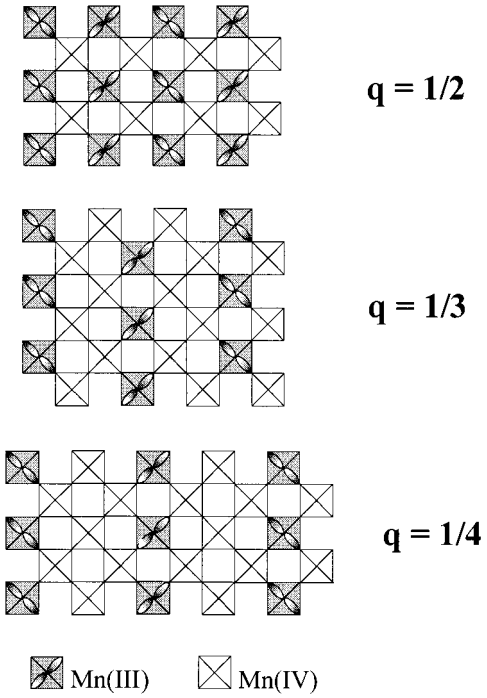

Figure 1. $Ln_{1-x}Ca_xMnO_3$: possible models of ordering of the Mn^{3+} and Mn^{4+} stripes proposed for rational *x* values: (a) $x = 1/2$ where one Mn^{3+} stripe alternates with one Mn^{4+} stripe; (b) $x = 2/3$ where one Mn^{3+} stripe alternates with two Mn^{4+} stripes; (c) $x = 3/4$ where one Mn^{3+} stripe alternates with three Mn^{4+} stripes.

Electron diffraction and transmission electron microscopy lattice images have also evidenced CO phenomena in $La_{1-x}Ca_xMnO_3$[11] and $Sm_{1-x}Ca_xMnO_3$[9] for various *x* values different from $1/2$. Long-range ordering was observed, involving a multiple cell "$1/q \times a_p\sqrt{2}$, $2a_p$,

(1) Kuwahara, H.; Tomioka, Y.; Asamitsu, A.; Moritomo, Y.; Tokura, Y. *Science* **1995**, *270*, 961.
(2) Wollan, E. O.; Koehler, W. C. *Phys. Rev.* **1955**, *100*, 545.
(3) Goodenough, J. B. *Phys. Rev.* **1955**, *100*, 564.
(4) Tomioka, Y.; Asamitsu, A.; Moritomo, Y.; Kuwahara, H.; Tokura, Y. *Phys. Rev. Lett.* **1995**, *74*, 5108.
(5) Chen, C. H.; Cheong, S. W. *Phys. Rev. Lett.* **1996**, *76*, 4042.
(6) Radaelli, P.; Cox, D. E.; Marezio, M.; Cheong, S. W. *Phys. Rev. B* **1997**, *55*, 3015.
(7) Jirak, Z.; Krupicka, S.; Simsa, Z.; Dlouha, M.; Vratislav, S. *J. Magn. Magn. Mater.* **1985**, *53*, 153.
(8) Damay, F.; Jirak, Z.; Hervieu, M.; Martin, C.; Maignan, A.; Raveau, B.; André, G.; Bourée, F. *J. Magn. Magn. Mater.* **1998**, *190*, 221.
(9) Hervieu, M.; Barnabé, A.; Martin, C.; Maignan, A.; Damay, F.; Raveau, B. *Eur. Phys. J. B*, **1999**, *8*, 31; *J. Mater. Chem.* **1998**, *8*, 1405.
(10) Millange, F.; de Brion, S.; Chouteau, G. *Phys. Rev. B* **2000**, *62*, 5619.

10.1021/cm000873s CCC: $20.00
Published on Web 03/22/2001

$a_p\sqrt{2}$", where $q \approx 1 - x$ characterizes the superstructure along $\vec{a}$. Models of commensurate ordering of the Mn^{3+} and Mn^{4+} stripes were proposed for rational x values as illustrated for $x = {}^2/_3$ where one Mn^{3+} stripe alternates with two Mn^{4+} stripes (Figure 1b) and for $x = {}^3/_4$ where one Mn^{3+} stripe alternates with three Mn^{4+} stripes (Figure 1c). An incommensurate ordering of these stripes was evidenced for irrational x values.[9,11]

In $Ln_{0.5}Sr_{0.5}MnO_3$ manganites, the size of the Ln cations plays a drastic role on the room-temperature structures, involving different types of cell distortions (*Pnma*, *Imma* or *I*2/*a*, *I*4/*mcm* or R$\bar{3}$c) as $\langle r_{Ln} \rangle$ increases. At low temperature, complex structural and magnetic coupled transitions are observed.[12−16] In the $Nd_{0.5}Sr_{0.5}MnO_3$, charge-ordering phenomena have been shown by electron diffraction[17] and confirmed by structural studies.[15−16]

In contrast to lanthanide manganites, the bismuth manganites $Bi_{1-x}A_xMnO_3$ (A = Ca, Sr) have been little studied, may be because of their lack of spectacular CMR properties.[18−20] Long period structures, associated with charge ordering, were indeed observed[20] for x ranging from 0.7 to 0.8. CO could compete with the ferromagnetic metallic state at low temperature to induce CMR properties that are only observed for the oxides $Bi_{1-x}Ca_xMnO_3$, for $x > 0.80$.[18]

To understand this different behavior of bismuth, it is of interest to investigate charge ordering phenomena in those oxides, especially if we take into account the abnormally high charge ordering temperature of 335 K reported for $Bi_{0.5}Ca_{0.5}MnO_3$.[21] The present electron microscopy study of the manganites $Bi_{1-x}Sr_xMnO_3$ evidences a new type of superstructure, associated with a charge ordering that is stable at RT and involving an original supercell. A model built up of double Mn^{3+} stripes alternating with double (denoted 2:2) and quadruple Mn^{4+} (2:4) stripes, respectively, is proposed. This type of charge order has never been reported to date, to our knowledge, in other manganites and may be at the origin of the abnormally high transition temperature $T_{CO} \approx 500$ K, observed for $Bi_{1/2}Sr_{1/2}MnO_3$. The considerable advantage of these samples is that, up to now, the observation of the CO phenomena by electron microscopy required the use of a cooling sample holder that hindered high-resolution images to be recorded.

Experimental Section

Starting from the cationic composition $Bi_{0.5}Sr_{0.5}Mn$, different types of synthesis were tested, varying the precursors of the solid-state reaction, the temperature, the oxygen content, and the atmosphere. Only the results obtained for two of these samples are reported herein. The first $Bi_{0.5}Sr_{0.5}MnO_{3+\delta}$ sample was prepared, starting from the peroxide SrO_2 and the oxides Bi_2O_3, and Mn_2O_3 in stoichiometric ratios. The mixture, intimately ground in an agate mortar, was pressed in the form of bars and sealed in a silica tube. It was heated at 1250 °C for 12 h. The temperature was slowly decreased down to 800 °C and the sample quenched to RT. The second sample was prepared, starting from $SrCO_3$, Bi_2O_3, and MnO_2, retaining the similar Sr/Bi/Mn ratio but working in air. The sample was heated at 1300 °C for 12 h, reground, and heated again at this temperature until a well-crystallized phase was obtained.

To compare the A-site cationic size effect on the charge ordering, thermal treatments, similar to the aforementioned ones, i.e., under air and in a silica tube, were used to prepare $Bi_{1-x}Ca_xMnO_3$ samples.

The powder X-ray diffraction analyses were carried out at RT with a Philips diffractometer working with the Cu Kα ($\lambda_1 = 1.5406$ Å and $\lambda_2 = 1.5443$ Å) in the range $10° \leq 2\theta \leq 110°$. The oxygen content was determined by chemical analyses.

For the electron microscopy study, small crystal flakes were deposited on a holey carbon film, supported by a copper grid. Electron diffraction (ED) study was carried out with JEOL 200CX and JEOL 2010 electron microscopes. Tilting around the crystallographic axes at RT and 92 K allowed reconstructing the reciprocal space. The high-resolution electron microscopy was carried out with a TOPCON 002B microscope ($V =$ 200 kV, Cs = 0.4 mm). Each of the microscopes is equipped with an energy dispersive spectroscopy (EDS) analyzer.

The resistivity measurements were performed from RT down to 5 K (in 0 and 7 K) by the four-probe method. The magnetization data were recorded using a Faraday balance.

Results

Sample Characterization. As mentioned in the Experimental Section, numerous samples have been prepared, varying the synthesis process. For most of the samples, the X-ray powder diffraction (XRPD) analysis show that a nearly single phased sample is obtained. The interesting point of this X-ray diffraction investigation deals with the fact that, starting from a given nominal composition, significant deviations of the cell parameters and the intensity of some of the reflections are observed in the patterns, depending on the experimental process that has been used. These results suggest that there exists a large existence range of the Bi-based perovskite manganite and that the structure is very sensitive to the cationic (i.e., x) and anionic content (i.e., δ).

The XRPD pattern of the sample obtained by working in sealed tubes, with an excess of oxygen (nominal oxygen content $O_{3.25}$), is given in Figure 2a. This X-ray pattern, indexed in a I-type cell (see next section on the symmetry), shows the sample is single phased. The EDS analyses carried out on numerous crystallites show that the actual composition is homogeneous and close to the nominal one, i.e., the cation content is $Bi_{0.5}Sr_{0.5}Mn$, in the limit of accuracy of the technique. Iodometric titration leads to an oxygen content close to O_3, in the accuracy limit of the technique. In the following, this pure sample is simply denoted $Bi_{0.5}Sr_{0.5}MnO_3$.

Working in air, from the same nominal composition, an isotypic compound formulated $Bi_{1-x}Sr_xMnO_3$ is obtained, but the EDS analysis evidences a bismuth loss

(11) Chen, C. H.; Cheong, S. W.; Hwang, H. Y. *J. Appl. Phys.* **1997**, *81*, 4326.
(12) Caignaert, V.; Millange, F.; Hervieu, M.; Suard, E.; Raveau, B. *Solid State Comm.* **1996**, *99*, 173.
(13) Morotomo, Y. Kwahara, H.; Tomioka, Y.; Tokura, Y. *Phys. Rev. B* **1997**, *55*, 7549.
(14) Damay, F.; Martin, C.; Hervieu, M.; Maignan, A.; Raveau, B.; André, G.; Bourée, F. *J. Magn. Magn. Mater.* **1998**, *184*, 74.
(15) Woodward, P. M.; Vogt, T.; Cox, D. E.; Arulraj, A.; Rao, C. N. R.; Karen, P.; Cheetham, A. K. *Chem. Mater.* **1998**, *10*, 3652.
(16) Woodward, P. M.; Cox, D. E.; Vogt, T.; Rao, C. N. R.; Cheetham, A. K. *Chem. Mater.* **1999**, *12*, 3528.
(17) Laffez, P.; VanTendeloo, G.; Millange, F.; Caignaert, V.; Hervieu, M.; Raveau, B. *Mater. Res. Bull.* **1996**, *31*, 905.
(18) Chiba, H.; Kikuchi, M.; Kusuba, K.; Muraoka, Y.; Syono, Y. *Solid State Comm.* **1996**, *99*, 499.
(19) Bao, W.; Axe, J. D.; Chen, C. H.; Cheong, S. W. *Phys. Rev. Lett.* **1997**, *78*, 543.
(20) Murakami, Y.; Shindo, D.; Chibo, H.; Kikuchi, M.; Syono, Y. *Phys. Rev. B* **1997**, *55*, 15043.
(21) Bokov, V. A.; Grigoryan, N. A.; Bryzhina, H. F. *Phys. Status Solidi* **1967**, *20*, 745.

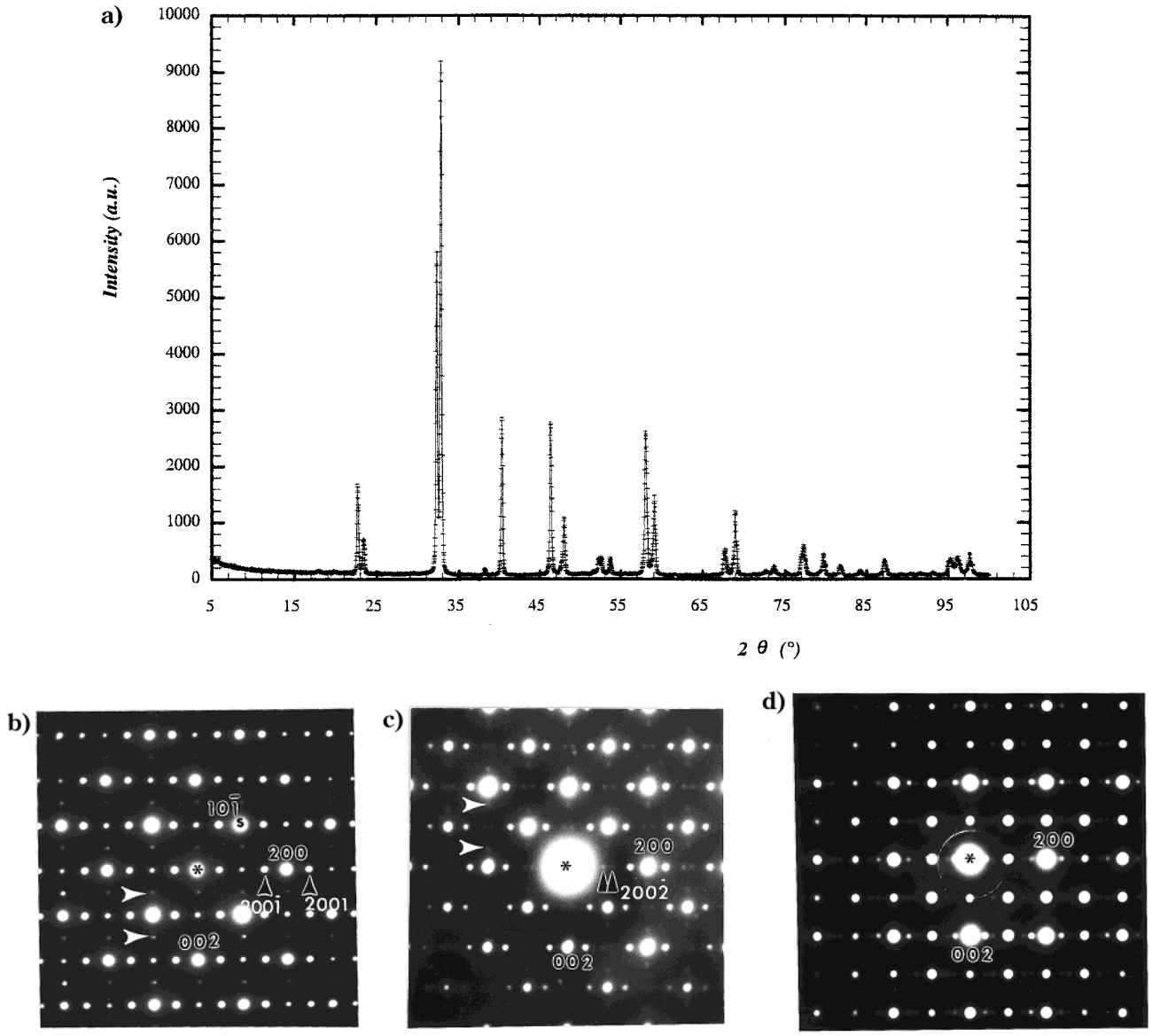

Figure 2. (a) XRPD pattern of $Bi_{0.5}Sr_{0.5}MnO_3$ synthesized in a sealed tube. [010] ED patterns, recorded at rt, for (b) $Bi_{0.5}Sr_{0.5}MnO_3$ and (c) $Bi_{0.44}Sr_{0.56}MnO_3$. The intense reflections *hkl* are indexed using black numbers (I-type subcell) and the satellites are indicated by the black arrows, using four white *hklm* indices. White arrows indicate the satellites belonging to the 90° oriented domains. (d) [010] ED patterns of $Bi_{0.4}$ $Ca_{0.6}MnO_3$ also exhibit satellites at rt (P-type subcell).

(actual bismuth content, $1 - x$, varying between 0.5 and 0.3). The electron diffraction characterization showed that this second sample contains an ill-crystallized impurity. Nevertheless, its investigation brings important information for charge-ordering phenomena.

Electron Diffraction. The electron diffraction study of the $Bi_{0.5}Sr_{0.5}MnO_3$ sample synthesized in an evacuated ampoule confirms that this oxide exhibits a perovskite-related structure. Characteristic ED patterns are given as examples in Figures 2b and 3. The reciprocal space of this compound consists of two sets of reflections:

(i) Intense reflections are characteristic of a quadruple perovskite cell with $a \approx a_p\sqrt{2} \approx 5.5$ Å, $b \approx 2a_p \approx 7.8$ Å, and $c \approx a_p\sqrt{2} \approx 5.5$ Å (a_p is the parameter of the cubic perovskite subcell). The angles α, β, and γ are very close to 90°. The reflection conditions *hkl*: $h + k + l = 2n$ show a centered I-type cell, similar to that observed for $Ln_{0.5}Sr_{0.5}MnO_3$ perovskites with Ln = La, Pr, and Nd,[4,12,14,15] which are either tetragonal (*I*4/*mcm*) or orthorhombic (*Imma*). In the $Bi_{0.5}Sr_{0.5}MnO_3$ sample, the presence of a second set of satellite reflections allow us to discard a tetragonal symmetry. The reflection conditions *hk*0: h, $k = 2n$, are compatible with the orthorhombic *Imma* and *Im*2*a* or the monoclinic *I*2/*a* space groups. The three space groups exhibit indeed exactly the same conditions limiting the reflection, and the differentiation could only be made by convergent beam electron diffraction. Keeping in mind these possible subtle differences, the *Imma* space group is taken into consideration in the present paper, and the systematic investigation of the actual symmetry of the series will be performed later.

(ii) Weaker extra spots are observed: they correspond to satellites in commensurate positions implying a doubling of the a parameter, so that the supercell parameters are $a_s \approx 2a_p\sqrt{2} \approx 11.11$ Å, $b_s \approx 2a_p \approx 7.83$ Å, and $c_s \approx a_p\sqrt{2} \approx 5.46$ Å (suffix s refers to the supercell). These satellites are rather intense for a majority of crystallites. Moreover, twinning domains are observed, as shown from the appearance of the satellites

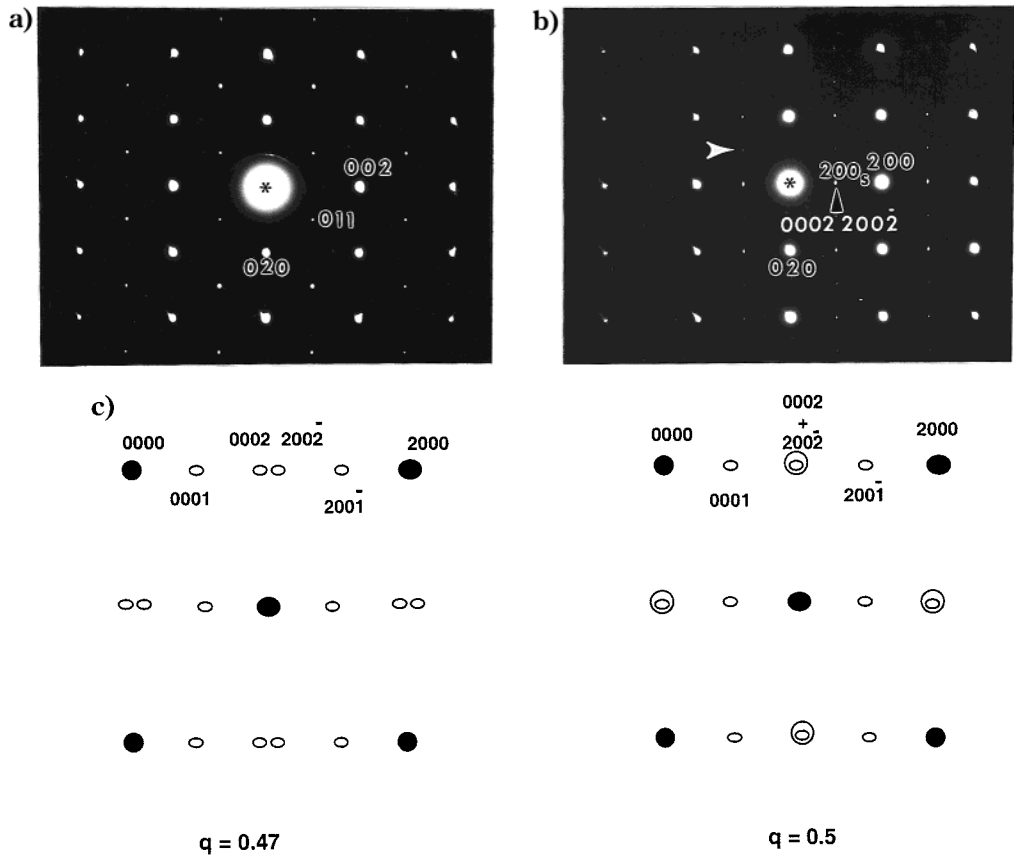

Figure 3. (a) [100] and (b) [001] ED patterns of $Sr_{0.5}Bi_{0.5}MnO_3$. **0002** and **200$\bar{2}$** satellites are superposed for $x = 1/2$. The white arrow indicates the presence of a small [100] oriented area in the [001] domain. (c) Schematic drawing and indexation (using *hklm*) of the [010] ED patterns for $q = 0.47$ and $q = 0.5$. Due to the superposition of **0002** and **200$\bar{2}$** satellites for $q = 0.5$, the pattern presents an apparent absence of reflection condition.

along two perpendicular directions (Figure 2b,c). This effect results from the pseudo-tetragonal character of the perovskite subcell and is systematically observed in the distorted perovskites.

Considering the [010], [100], and [001] ED patterns of $Bi_{0.5}Sr_{0.5}MnO_3$ (Figures 2b and 3), unusual extinction conditions must be outlined. For this compound, the basal ED pattern (Figure 2b) cell could suggest that the I-type lattice might be lowered to a P-type lattice due to the absence of reflection conditions for h_s0l_s (the **10$\bar{1}$**$_s$ reflection is indexed in the "$2a_p\sqrt{2} \times 2a_p \times a_p\sqrt{2}$" cell). In contrast, the reconstruction of the reciprocal space, carried out for numerous crystallites, supports the I-type symmetry. The structure factors of the $h_sk_sl_s$: $h_s + k_s + l_s \neq 2n$ reflections, i.e., those which violate the I-type symmetry, are nil or so weak that they are not visible in the ED patterns (except for the h_s0l_s namely for $k_s = 0$). In the [100] and [001] basal ED patterns, the reflection conditions $0k_sl_s$: $k_s + l_s = 2n$ and h_sk_s0: h_s, $k_s = 2n$ are observed.

The ED study of the second sample, $Bi_{1-x}Sr_xMnO_3$, for which crystallites exhibit various x values different from $x = 1/2$ ranging from $x = 0.51$ up to $x = 0.67$, allows the above unusual extinction conditions to be understood. The first information concerns the extra reflections, which are shown to be in incommensurate positions as soon as x is different from 0.5. This result is important for the following reasons:

(i) An incommensurate modulated structure is observed for the first time in the Sr-based manganites $Ln_{1-x}Sr_xMnO_3$. Up to now, all the results show that, in these compounds, the CO only involves a commensurate structure with a doubling of the ***a*** parameter.

(ii) The fact that the structure is modulated allows understanding the aforementioned unusual conditions of reflection. It indeed explains the discrepancy between the apparent absence of reflection conditions (P-type) in the basal planes and the observation in the reconstruction of the reciprocal space. This is schematized in Figure 3c, drawing two theoretical [010] patterns with the same I-type subcell but different q values, namely $q = 0.47$ and $q = 0.5$. The superposition of the **0002** and **200$\bar{2}$** satellites leads to an apparent absence of reflection conditions. $Bi_{0.5}Sr_{0.5}MnO_3$ is only a particular point of the $Bi_{1-x}Sr_xMnO_3$ series. The modulation vector is parallel to a^*, regardless of x. The component q of the modulation vector **a*** is rational, $q = 0.5$, for $Bi_{0.5}Sr_{0.5}MnO_3$ and irrational for other x values of $Bi_{1-x}Sr_xMnO_3$. Moreover, the q value roughly follows the x value ($q \approx 1 - x$). This is illustrated by the [010] ED patterns of one $Bi_{0.5}Sr_{0.5}MnO_3$ crystallite (Figure 2b) and one $Bi_{1-x}Sr_xMnO_3$ crystallite (Figure 2c) with $x \approx 0.56$ (determined by EDS). For $x \neq 1/2$, it clearly appears that the satellites, which are in incommensurate positions, are associated with a system of reflections of an I-type centered lattice. The ED patterns can then be indexed using four *hklm* indices (white numbers in Figure 2) with a wave vector **qa***, and the conditions limiting the reflections are *hklm*: $h + k + l = 2n \; \forall \; m$

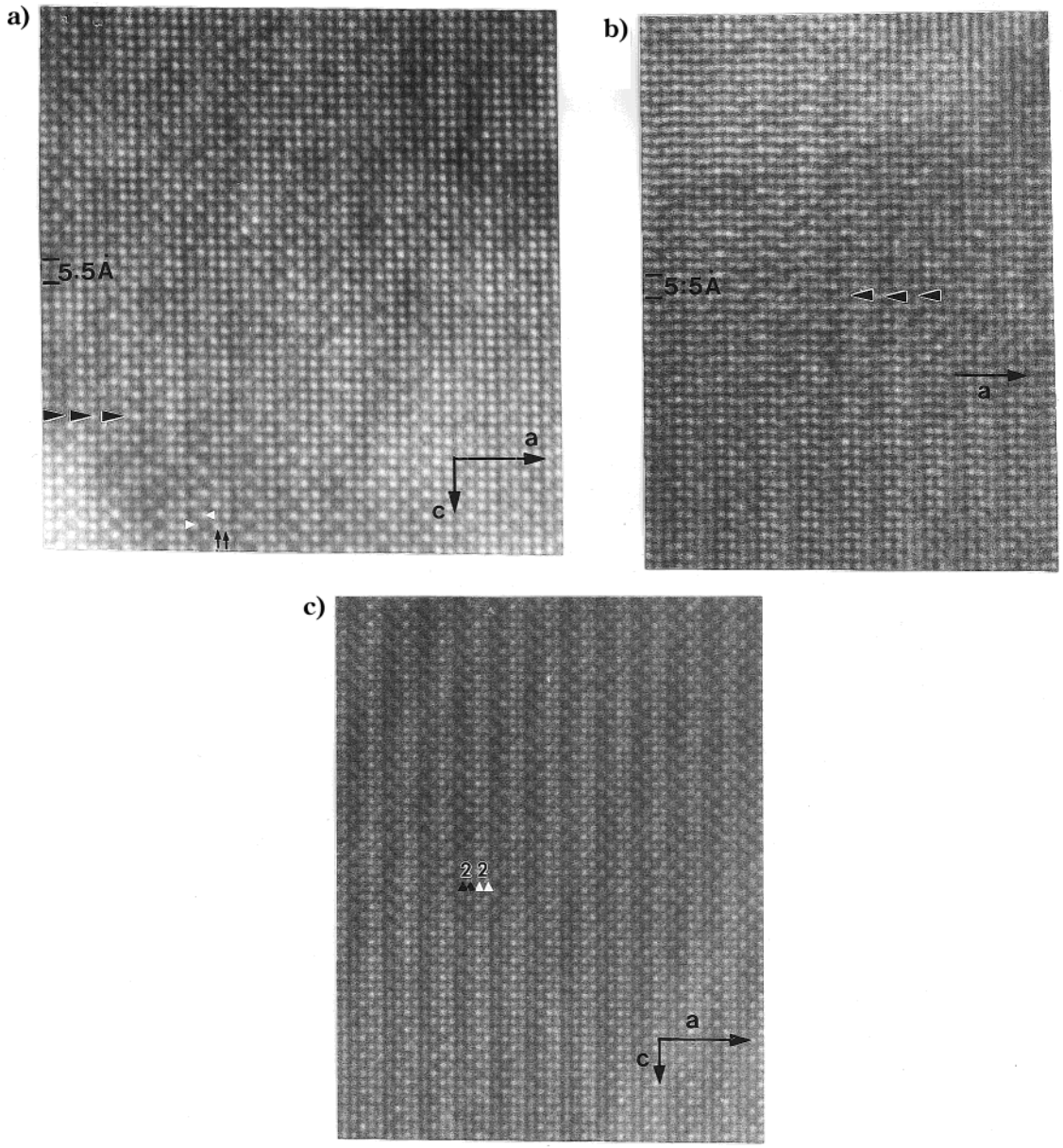

Figure 4. [010] HREM images of $Bi_{0.5}Sr_{0.5}MnO_3$ (a) on the very thin edge of the crystallite, ($\Delta f \approx -50$ nm). Two small black arrows and two white triangles indicate the two types of contrast observed in the double rows of white spots and the waving effect by the dark triangles. (b) The waving effect clearly appears for a slight variation of the focus value. (c) Thick part of the crystal where the "**2 + 2**" contrast modulation is very regularly established.

and $hk0m$: $h + m = 2n$, involving ***Imma* (α00) 00s** as super space group.

These important points merit comments. The first one deals with the comparison between the cell symmetry of the $Ln_{0.5}Sr_{0.5}MnO_3$ (Ln = La, Pr, and Nd) and $Bi_{0.5}Sr_{0.5}MnO_3$ manganites, at RT. All these manganites exhibit a I-type symmetry, but they show a fundamental difference: at RT, the $Ln_{0.5}Sr_{0.5}MnO_3$ are in the paramagnetic state, contrary to the ordered $Bi_{0.5}Sr_{0.5}MnO_3$ for which $T_{CO} \approx 500K > RT$ (see the last section). Note that, from the simple cation size point of view,[15] an I-type structure is also expected for $Bi_{0.5}Sr_{0.5}MnO_3$ above 500K. The second point, closely related, deals with the nature of the CO, which cannot be compared for $La_{0.5}Sr_{0.5}MnO_3$ and $Pr_{0.5}Sr_{0.5}MnO_3$ since they are not ordered.

To allow a significant comparison, we have synthesized $Bi_{1-x}Ca_xMnO_3$ ($0.6 \geq x \geq 0.4$) samples, which are also characterized by a T_{CO} higher than RT. A typical [010] ED pattern of $Bi_{0.4}Ca_{0.6}MnO_3$, recorded at RT, is given in Figure 2d, which is to be compared with Figure 2b. It also exhibits an incommensurate modulated structure. It clearly appears that the *Pnma*-type system of intense reflections (*h0l*: no cond.) remains intense and is associated to a system of satellites which involves $q \approx 0.4$. This result is consistent with those reported in refs 15, 18 for $Bi_{0.2}Ca_{0.8}MnO_3$, and shows, important, that the $Bi_{1-x}Ca_xMnO_3$ manganites behave like $Ln_{1-x}Ca_xMnO_3$,[5-9] the modulation vectors following the x values. The comparison between the two [010] ED patterns clearly shows that the satellites associated to the Bragg reflections of the perovskite subcell, keep unchanged this P− or I− type subcell symmetry, which is directly correlated to the octahedra tilt and distortion system. These results clearly imply that, below T_{CO}, different types of charge ordering effect would exist. Due

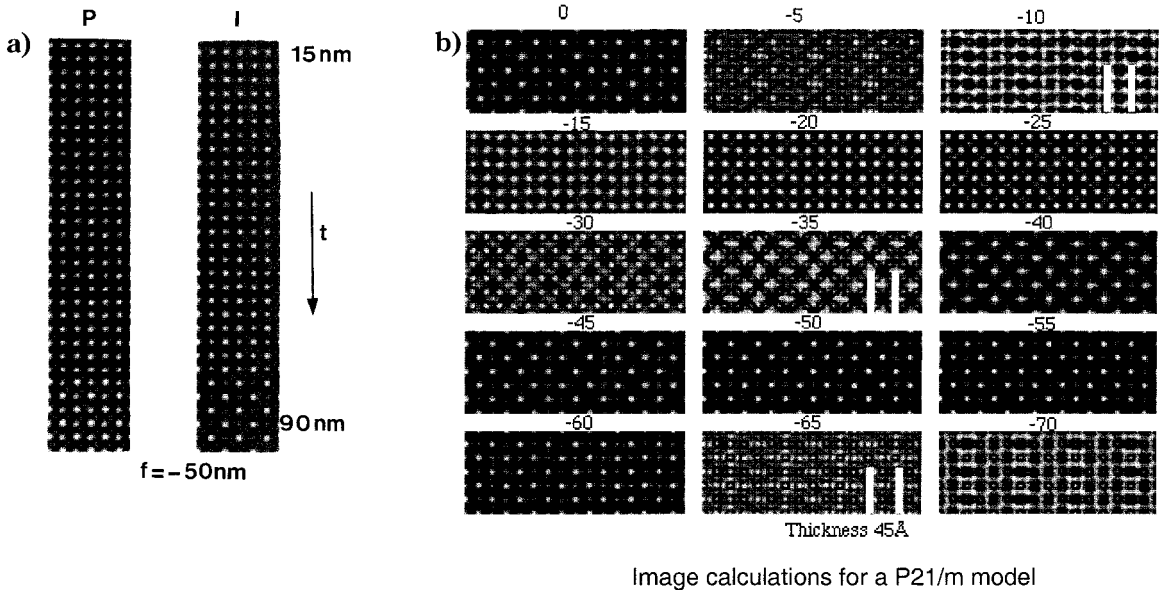

Figure 5. (a) Simulated image calculated for a focus value ≈ -50 nm and a thickness range 15 Å $\leq t \leq$ 90 Å: P-type structure and I-type structure. (b) Simulated through focus series, calculated for a "$P2_1/m$" type of charge ordering. The thickness is 4.5 nm. The vertical white bars are a guide for the eyes to indicate the sequence, along **a**, of the dots' brightness.

to the high T_{CO} value, the structure of the ordered $Bi_{1-x}Sr_xMnO_3$ samples can be investigated using high-resolution electron microscopy at RT.

High-Resolution Electron Microscopy. The electron diffraction investigation of the two $Bi_{0.5}Sr_{0.5}MnO_3$ and $Bi_{1-x}Sr_xMnO_3$ samples shows that the perovskite phases exhibit, at RT, a modulated structure over a rather large domain of existence, which can be compared to that observed at low temperature for charge-ordered manganites $Ln_{1-x}Ca_xMnO_3$.[10-11] To understand these modulation effects and especially their relations with the possible ordering of Mn^{3+} and Mn^{4+} species, we have performed a high-resolution electron microscopy study of the two types of samples, selecting the [010] orientation. [010] HREM images of $Bi_{0.5}Sr_{0.5}MnO_3$ are given in Figure 4.

In Figure 4a, recorded on the very thin edge of the crystallite, the bright spots are correlated to the high electron density areas (focus value estimated to be close to -50 nm). In the lower part of this image, one observes the formation of two types of double rows of white dots running along c: two adjacent rows of spots of equal brightness (see the two small black arrows) alternating with two rows of bright and less bright spots in staggered positions (see the two white triangles). Concomitantly, one observes an undulation of the rows running along a: this effect is clearly seen by viewing at grazing incidence along the dark triangles. It is more straightforward for a slight variation of the focus value, as shown in Figure 4b, where the two types of double rows are also clearly visible. Increasing the crystallite thickness, the contrast slightly evolves, as shown in Figure 4c, where the "**2** + **2**" contrast modulation of the two types of double rows is very regularly established.

Two different hypotheses are susceptible to explain the presence of such double bright rows: either a 1:1 Sr/Bi ordering or a 1:1 Mn^{3+}/Mn^{4+} charge ordering. The above experimental images compared to the theoretical ones calculated for Bi/Sr ordering show without ambiguity that the Bi^{3+} and Sr^{2+} cations are distributed at random over the A sites. This observation is in agreement with the electron diffraction study carried out warming the sample (see the discussion). On the opposite, the contrast variations experimentally observed can, in fact, be compared to those observed by simply varying the octahedral framework distortion. The distortion effect is illustrated in Figure 5a. Two series of theoretical images are calculated for the same composition $Bi_{0.5}Sr_{0.5}MnO_3$, considering one P-type and one I-type tilting mode: only one focus value close to -50 nm (heavy electron density areas in bright) is considered, but the crystal thickness is varied from 15 to 90 nm. It clearly shows that these small distortions are sufficient to generate the experimental contrast variations, see for example the rows of equal brightness dots and those in staggered positions for the thicker part of the crystal (bottom part of the images in Figure 5a).

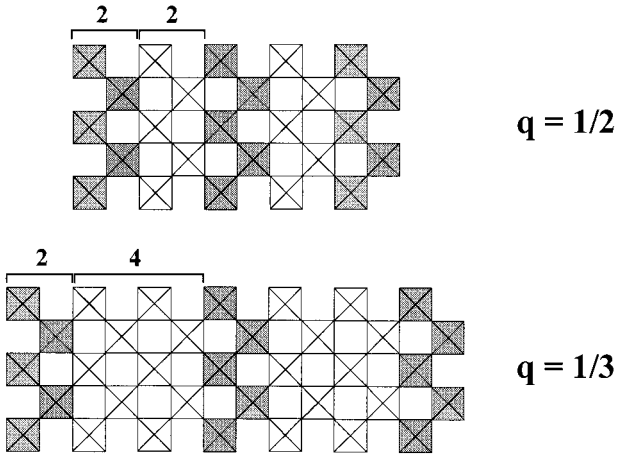

Figure 6. Ideal model of a double stripelike ordering: (a) "**2** + **2**" and (b) "**2** + **4**".

The hypothesis of the regular alternation along **a** of two types of double rows ("**2** + **2**" contrast modulation) is reinforced by the small increase in the spacing between the rows is in favor of the formation of a double row of slightly larger octahedra. This suggests that the modulations are correlated to tiny displacements of the atoms which occur in the form of double rows of a first

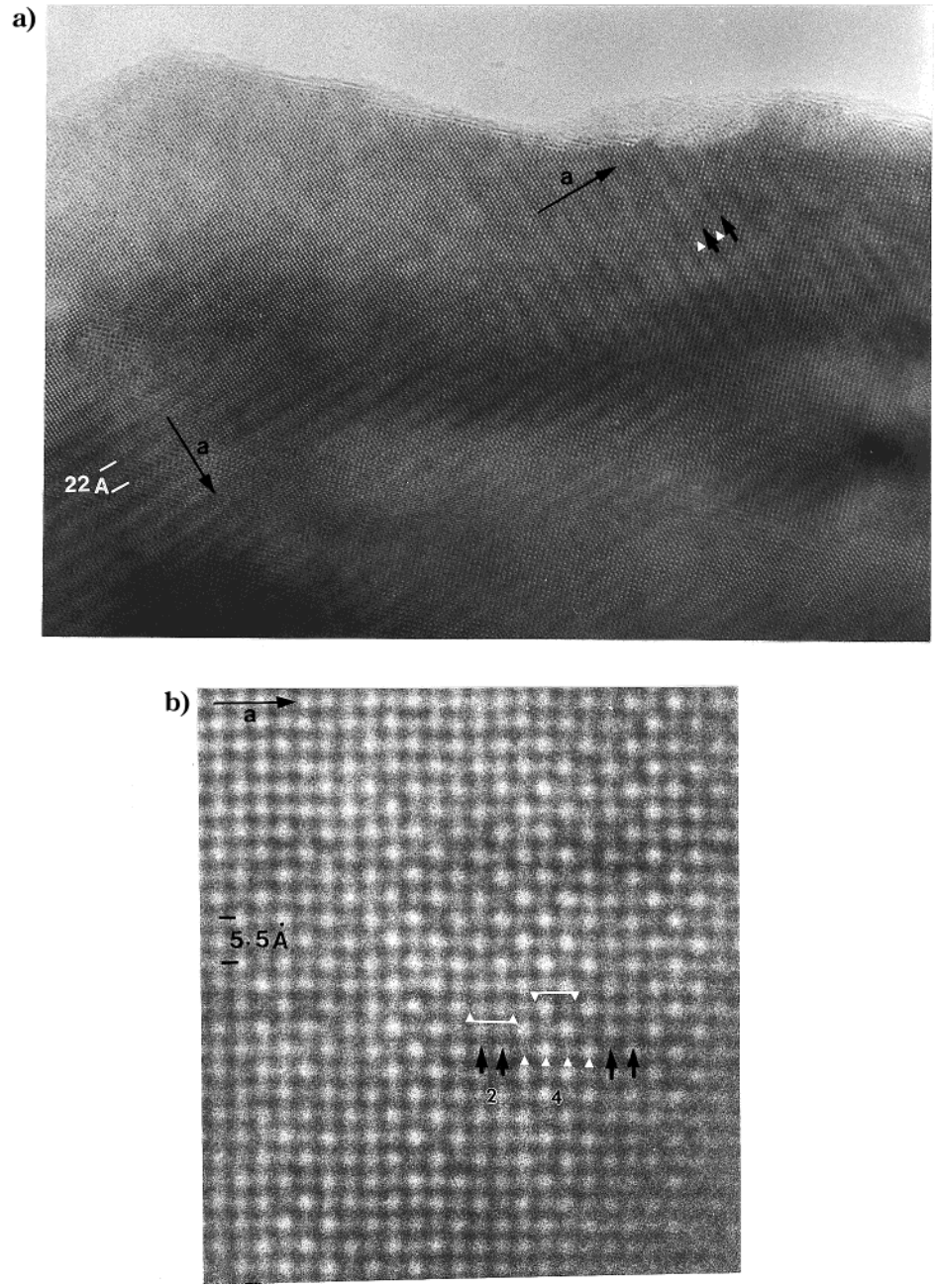

Figure 7. [010] HREM images recorded for a $Bi_{0.33}Sr_{0.67}MnO_3$: (a) overall image and (b) enlarged image. Small black arrows indicate double row of equally bright spots and small white triangles the bright spots in staggered positions (I-type contrast).

type of MnO_6 octahedra alternating with double rows of a second type of MnO_6 octahedra. A model which consists of double stripes of Mn^{3+} octahedra (larger size and distortions) alternating with double stripes of Mn^{4+} octahedra is proposed in Figure 6a. This model is indeed different from the one proposed for the $Ln_{0.5}Ca_{0.5}MnO_3$ and $Nd_{0.5}Sr_{0.5}MnO_3$ compounds (proposed by Jirak[7]). For checking our interpretation of the image contrast, calculations were carried out using the positional parameters refined from neutron diffraction data by Woodward et al.[15] for the ordered form of $Nd_{0.5}Sr_{0.5}MnO_3$. The calculated focus series is given in Figure 5b, for a crystal thickness close to 4.5 nm. One clearly observes that this model does not involve contrast variations in the form of the "**2** + **2**" contrast modulation that we observe. White lines added to the image (Figure 5b) for a focus value of −10 nm show that the contrast modulation could be described by the following sequence of the dots brightness along **a**: bright − gray − dark − gray, sequence which is in agreement with the $P2_1/m$ model.

The existence of a double ribbon model (2:2) of charge ordering is supported also by the observations carried out on the second sample. Figure 7 presents [010] images recorded for a similar focus value (overall image in Figure 7a and enlarged image in Figure 7b). The EDS analysis evidences a $Bi_{0.33}Sr_{0.67}MnO_3$ composition ($x \approx {}^2/_3$), and the ED diffraction pattern shows that the component of the modulation vector along **a*** is $q \approx {}^1/_3$; i.e., the parameter of the supercell is $3a_p\sqrt{2}$. The way the contrast varies is similar, in principle, to that observed in the $Bi_{0.5}Sr_{0.5}MnO_3$ sample and simply varies in its periodicity. A double row of bright spots of equal brightness (small black arrows) alternates along **a**, with

a quadruple row of bright and less bright spots in staggered positions (small white triangles). Viewing at grazing incidence along a evidences also a small periodic undulation of the rows. The "**2** + **4**" periodicity is nearly regularly established over the whole crystal. The small linear white segments drawn in Figure 7b show that the spacing between the double rows of equal brightness is slightly longer (with triangle apex up) than the one observed in the quadruple rows (triangle apex down). Taking into consideration the image calculations which show that the Bi/Sr ordering must be ruled out, these observations are consistent with a stripe model for the manganite $Bi_{1/3}Sr_{2/3}MnO_3$, in which one Mn^{3+} double stripe alternates with one Mn^{4+} quadruple stripe (Figure 6b).

Discussion

This electron microscopy study shows for the first time charge ordering (CO) phenomena at RT in manganites, using high-resolution microscopy, since to date only lattice images could be obtained, due to the techniques of observations at low temperature. The CO phenomena as observed in $Bi_{1-x}Sr_xMnO_3$ differ fundamentally from those observed in lanthanide manganites $Ln_{1-x}Ca_xMnO_3$[9−10] and could be explained by a structural model made of double "Mn^{3+}" stripes alternating with multiple "Mn^{4+}" stripes (Figure 6), whereas single "Mn^{3+}" stripes alternating with multiple "Mn^{4+}" are observed for $Ln_{1-x}Ca_xMnO_3$ (Figure 1). Similarly the centered I-type symmetry of the $Bi_{1-x}Sr_xMnO_3$ manganites is different from the P-type symmetry observed for the charge ordered $Ln_{1-x}Ca_xMnO_3$ manganites and from that observed in the $Pr_{0.5}Sr_{0.41}Ca_{0.09}MnO_3$.[22]

This new kind of charge ordering observed for $Bi_{0.5}Sr_{0.5}MnO_3$ and $Bi_{0.33}Sr_{0.67}MnO_3$ raises the question of the influence of the $6s^2$ lone pair stereoactivity of Bi^{3+} upon such a phenomenon. The absence of Bi/Sr and Bi/Ca ordering supports the hypothesis that the Bi^{3+} lone pair is not the main responsible.

Finally, the last remarkable feature of $Bi_{0.5}Sr_{0.5}MnO_3$ deals with its very high charge ordering temperature T_{CO}, despite the large average size of the A-site cations. The reciprocal susceptibility curve $1/\chi(T)$ (Figure 8a) shows indeed that T_{CO} is the highest that has been observed to date in manganites. The electron diffraction of the $Bi_{0.5}Sr_{0.5}MnO_3$ sample was carried out vs T, warming the sample up to 550 K. One observes that the extra reflections disappear at a temperature close to 500 K. More important, the effect is reversible and the satellites re-appear by cooling to RT. This observation supports that the satellites are not generated by a Bi/Sr ordering but are correlated to a charge/orbital phenomenon, in agreement with the magnetic measurements. The second change of slope on the $1/\chi(T)$ curve around 190 K might be correlated with T_N. The signature of CO cannot be seen on the $\rho(T)$ curve (Figure 8b), since our measurements could only be performed up to 400 K, i.e., below T_{CO}. Moreover, it must also be noticed that this compound is not magnetoresistive, suggesting that the charge ordered state is very stable and cannot be melted up to 7T.

In summary, a new kind of charge ordering has been observed with an exceptional stability, T_{CO} reaching 500

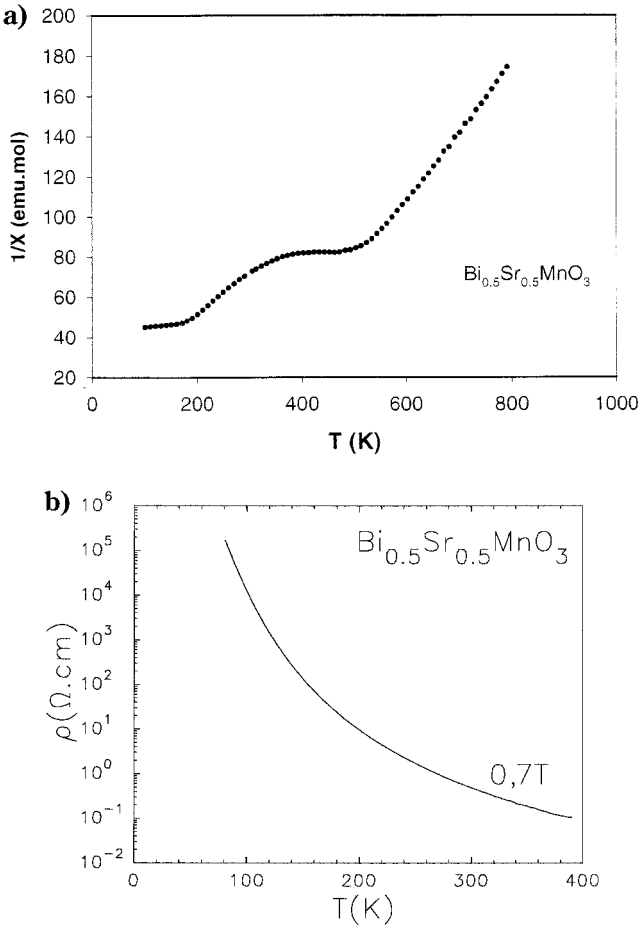

Figure 8. $Bi_{0.5}Sr_{0.5}MnO_3$: (a) reciprocal susceptibility curve $1/\chi(T)$ and (b) $\rho(T)$ curve.

K. These results raise also numerous questions. The first one is indeed to carry out the crystal structure refinements from X-ray and neutron diffraction data, to understand the octahedra tilting and distortion in our samples. It is also important to determine the magnetic structure since, in a recent brief report,[23] Frontera et al. report the coexistence of two different antiferromagnetic A and CE phases in two compounds of the $Bi_{1-x}Sr_xMnO_3$ series. The CO in the $P2_1/m$ or in other structural types[22] of the $Ln_{0.5}A_{0.5}MnO_3$ manganites at low temperature has been correlated to CE-type antiferromagnetic phases. The CE-AFM model is consistent with the fact that all these phases exhibit commensurate modulation, with a doubling of the **a** parameter. Consequently, the "ideal" CE-type spin ordering is not consistent with an incommensurate modulated phase. The magnetic structures of these complex compounds are thus far to be understood, and a lot of work has to be done. Last, this study shows that the system is very rich and that different phases can be stabilized depending on the nominal composition and synthesis process. Further investigations have to be carried out to determine the role of the $6s^2$ lone pair of Bi^{3+} upon the appearance of double Mn^{3+} stripes in this oxide and to understand the relationship between its structure and magnetic properties.

CM000873S

(22) Damay, F.; Zirak, Z.; Hervieu, M.; Martin, C.; Maignan, A.; Raveau, B. *J. Magn. Magn. Mater.* **1998**, *190*, 221.

(23) Frontera, C.; Llobet, A.; Garcia-Aranda, M. A.; Ritter, C.; Garcia-Munoz, J. L. *Physica B* **2000**, *276*, 793.